

Background galaxies as reddening probes throughout the Magellanic Clouds

C.M. Dutra^{1,3}, E. Bica^{1,3}, J.J. Clariá^{2,3}, A.E. Piatti^{2,3} and A.V. Ahumada^{2,3}

¹ Instituto de Física-UFRGS, CP 15051, CEP 91501-970 POA - RS, Brazil

² Observatorio Astronómico de Córdoba, Laprida 854, 5000, Córdoba, Argentina

³ Visiting Astronomer, Complejo Astronómico El Leoncito operated under agreement between the Consejo Nacional de Investigaciones Científicas y Técnicas de la República Argentina and the National Universities of La Plata, Córdoba and San Juan.

Received; accepted

Abstract. We study the spectral properties in the range 3600Å - 6800Å of the nuclear region of galaxies behind the Magellanic Clouds. The radial velocities clarified the nature of the objects as background galaxies or extended objects belonging to the Clouds. For most galaxies behind the main bodies of the LMC and SMC, radial velocities were measured for the first time. In the present sample typical LMC background galaxies are nearby ($4000 < V(\text{km/s}) < 6000$), while SMC's are considerably more distant ($10000 < V(\text{km/s}) < 20000$). We determine the reddening in each line of sight by matching a reddening-free galaxy template with comparable stellar population. For the LMC main body we derive a combined Milky Way and internal reddening value $E(B-V)_{MW+i} = 0.12 \pm 0.10$, while for the SMC $E(B-V)_{MW+i} = 0.05 \pm 0.05$. By subtracting Milky Way reddening values for galaxies projected onto the surroundings of each Cloud, we estimate average internal reddening values $\Delta E(B-V)_i = 0.06$ and 0.04 , respectively for the main bodies of the LMC and SMC. The Clouds are optically thin, at least in the directions of the studied background galaxies which are often difficult to be identified as such on ESO/SERC sky survey images. Nevertheless, more reddened zones may occur where it is difficult to identify galaxies.

Key words: ISM: dust, extinction – Galaxy: general – Galaxies: Magellanic Clouds, ISM, stellar content

1. INTRODUCTION

The galactic reddening distribution was initially modeled as a function of galactic latitude in terms of a Coscant Law (Sandage 1973 and references therein). A dependence on galactic longitude was derived by de Vaucouleurs et al. (1976). The polar cap zero points have been a matter of debate with estimates ranging from reddening free to

$E(B-V)=0.05$. These models do not take into account local reddening variations, since the dust distribution can be very patchy, including high galactic latitudes where many discrete clouds occur (e.g. Reach et al. 1998). The empirical formulation by Burstein & Heiles (1978, 1982) improved the reddening distribution description by relating HI column density and galaxy counts to reddening. Nevertheless the HI and dust contents do not scale in the same way everywhere, in particular in cold dense clouds where hydrogen becomes mostly molecular.

Recently, Schlegel et al. (1998, hereafter SFD98) provided a new estimator of galactic reddening by means of a full-sky 100 μm IRAS/ISSA map which was converted to dust column density by using a dust colour temperature map (17°K to 21°K) derived from 100 and 240 μm COBE/DIRBE maps. The dust emission map is calibrated in terms of $E(B-V)$ reddening values using determinations from early type galaxies by means of the $(B-V)$ vs $\text{Mg}2$ relation. SFD98's dust emission reddening $E(B-V)_{FIR}$ appears to be sensitive to the dust content of the cold dense clouds and their accumulation in different lines of sight. Dutra & Bica (2000) compared $E(B-V)_{FIR}$ values with the reddening $E(B-V)$ measured from the stellar content of globular and old open clusters in the Galaxy. It was concluded that differences between these reddening values most probably arise from dust distribution in the cluster foreground and background.

The stellar content of background galaxies offers an opportunity to analyse the total Milky Way dust column in a given line of sight, as well as those of the Magellanic Clouds. Recently the NED database included a facility tool to determine SFD98's $E(B-V)_{FIR}$ in any direction. However for the main bodies of the LMC and SMC NED adopted uniform foreground reddening values of $E(B-V)_{FIR} = 0.075$ and $E(B-V)_{FIR} = 0.037$, respectively. These values are from the average dust emission in their surroundings (SFD98). We emphasize that in the present study we use SFD98's original facility tool (`dust-getval.f`) and the whole sky dust emission reddening

maps, which include the internal dust emission structure of the LMC and SMC $E(B-V)_{FIR}$ maps. As pointed out by SFD98 they have not analysed the $E(B-V)_{FIR}$ values in the Clouds.

The Magellanic Clouds cover a significant portion of the sky and their background galaxies have not yet been studied in detail due in part to reddening and crowding effects. Oestreicher et al. (1995) mapped the galactic reddening in the direction of the LMC by means of UVB photometry of foreground galactic stars. They obtained a mean reddening of $E(B-V)_{MW} = 0.06 \pm 0.02$. For the SMC the mean foreground reddening is $E(B-V)_{MW} \approx 0.03$ considering colour-magnitude diagrams of clusters in the outer parts of the SMC such as K3, L1 and NGC121 (Westerlund 1990). Oestreicher & Schmidt-Kaler (1996) studied the internal reddening distribution of the LMC with dust clouds in the range $0.04 < E(B-V)_i < 0.40$. Reddening estimates using background galaxies by means of count methods have been applied for the SMC (Wesselink 1961, Hodge 1974, MacGillivray 1975) and LMC (Gurwell & Hodge 1990). These studies provide very high reddening values in some regions which seem to arise from count losses owing to star crowded fields and extended objects belonging to the Clouds.

In the present study, we observe and analyse integrated spectra of nuclear regions of galaxies behind the main bodies of the Clouds to probe reddening in those lines of sight. We take into account different stellar populations by using template spectra. For comparison purposes we also observed galaxy spectra in the surroundings of the Clouds and towards the Galactic South Polar Cap. In Sect. 2 we present the samples in the directions of the Clouds and South Polar Cap. In Sect. 3 we describe the observations and reductions. In Sect. 4 we establish the nature of the objects. Most of them turn out to be galaxies, but some are extended objects belonging to the Clouds. In Sect. 5 we compare the present galaxy spectra with those of stellar population templates from Bica (1988, hereafter B88), and provide some new templates as well. In Sect. 6 we derive the reddening value for each galaxy behind the Magellanic Clouds and discuss their distribution and overall transparency of the Clouds. Concluding remarks are given in Sect. 7.

2. The samples

In the main bodies of the Magellanic Clouds it is often difficult to establish the morphological type of a galaxy using ESO/SERC Schmidt plates and Digitized Sky Survey atlases. In some cases is not possible to distinguish a galaxy from an extended object belonging to the Clouds, such as a compact H II region or star cluster.

2.1. Objects towards the Magellanic Clouds

We selected galaxies behind the Magellanic Clouds and also included objects with uncertain classification and/or excluded from the revised and extended catalogues of extended objects in the SMC (Bica & Schmitt 1995, Bica & Dutra 2000) and LMC (Bica et al. 1999) to establish their nature. These LMC or SMC main body objects are: (i) SMC-DEM92(AM0054-744ne), LMC-DEM225 and LMC-DEM329 from the SMC and LMC catalogues of emission nebulae by Davies et al. (1976); (ii) HS75-8, HS75-10, HS75-13, HS75-18, HS75-20, HS75-22, HS75-23 and HS75-25 from the catalogue of galaxies behind the SMC by Hodge & Snow (1975); (iii) HS17, HS45, HS257, HS356, HS394, HS449 and HS451 from the LMC star cluster catalogue by Hodge & Sexton (1966); (iv) SL887 from the LMC star cluster catalogue by Shapley & Lindsay (1963); (v) OHSC3 from the LMC star cluster catalogue by Olszewski et al. (1988); and (vi) HW60 from the SMC star cluster catalogue by Hodge & Wright (1974).

Figures 1 and 2 show the angular distribution of the observed objects towards the SMC and LMC respectively. We distinguish the literature galaxies that we observed (LEDA and/or NED extragalactic databases) from the objects whose nature will be established in the present study. The latter objects are excellent reddening probes for the central regions of the Clouds. A preliminary discussion of part of the Magellanic Clouds sample was given in Dutra et al. (1998).

The 43 selected objects are presented in Table 1, by columns: (1) designation, (2) and (3) J2000 equatorial coordinates, (4) and (5) galactic coordinates, (6) total magnitude B_T (LEDA/NED), (7) exposure time, (8) radial velocity measurement, (9) LEDA and/or NED radial velocity, and (10) LEDA/NED morphological type or estimated by ourselves on ESO/SERC plates when possible. Additional objects included in Table 1 are discussed subsequently.

2.2. South Polar Cap

The South Polar Cap sample ($b < -70^\circ$) consists of 13 early type galaxies to minimize stellar population variations. SFD98 pointed out the existence of low reddening regions between cirrus filaments near the Galactic Poles, and in some regions outside the Polar Caps as well at intermediate latitudes. Some of the latter regions have $E(B-V)_{FIR}$ values four times less than those estimated for the Polar Caps averaged over regions of diameter 10° , which are $E(B-V)_{FIR} = 0.015$ and 0.018 , respectively for the Northern and Southern Polar Caps. We observed these galaxies to create reddening-free galaxy templates under the same observational conditions as the Magellanic Clouds sample. We also observed 9 intermediate galactic latitude galaxies ($-64^\circ < b < -29^\circ$) which are in common with those in B88's red stellar population templates in early type

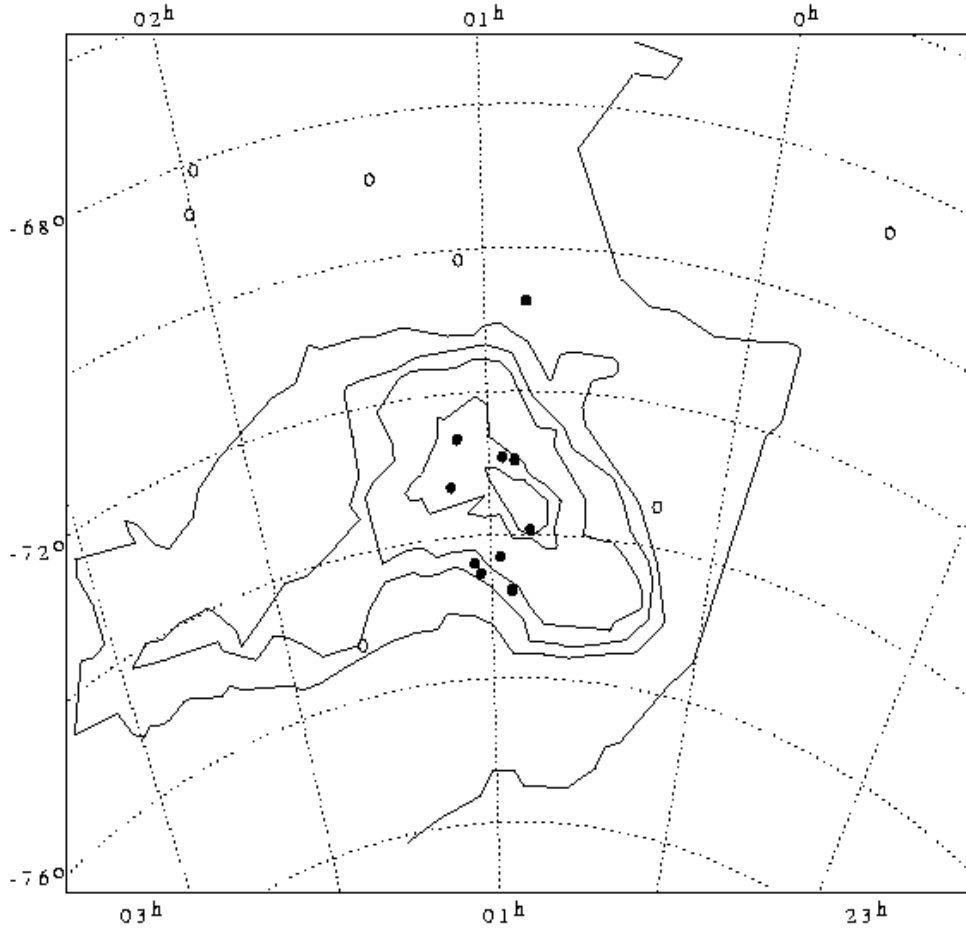


Fig. 1. Angular distribution of the observed SMC background known galaxies (open circles) and candidate galaxies (filled circles). The solid lines represent HI contours of 5, 50, 100, 150, 400 and 600 in units $10^{19} \text{ atoms cm}^{-2}$ from Mathewson & Ford (1984).

galaxies. The latter galaxies were observed for comparison purposes. The samples are given in Table 1.

3. Observations and reductions

The spectra were collected with the 2.15-meter telescope at the Complejo Astronómico El Leoncito (CASLEO, San Juan, Argentina) in December 1995 and October 1998. We employed a CCD camera attached to the REOSC spectrograph. The detector was a Tektronics chip of 1024×1024 pixels of size $24\mu \times 24\mu$. We used a grating of 300 grooves mm^{-1} producing an average dispersion of $\approx 143\text{\AA}/\text{mm}$ or $3.43\text{\AA}/\text{pixel}$. The spectral coverage was $3600\text{\AA} - 6800\text{\AA}$. At least two exposures of each object were taken in order to correct for cosmic rays. The exposure times are given in Table 1. The standard stars EG21 and LTT3864 (Baldwin & Stone 1984) were observed for flux calibrations. He-Ne lamp exposures were taken following that of the object or

standard star for wavelength calibrations. The slit width was $4''$ providing a resolution (FWHM) of $\approx 14\text{\AA}$ from comparison lines. The slit was set in the E-W direction, and its length projected on the chip ($4.7'$) provided a wide range of pixel rows for background subtractions.

The reductions were carried out at the Instituto de Física, UFRGS (Porto Alegre - Brazil) and Observatorio Astronómico, Universidad Nacional de Córdoba (Córdoba - Argentina), with the **IRAF** package following standard procedures. The galaxy spectra were extracted along the slit according to the dimensions of each galaxy nuclear region. Typical extractions were $\approx 8\text{-}10''$.

Since the spectral resolution was chosen for stellar population purposes, it is not ideal for velocity measurements. At any rate, we measured velocities and the agreement with values in common with the literature is good (Table 1). In one case, ESO28G12, the current LEDA and NED velocities are significantly different, and the present obser-

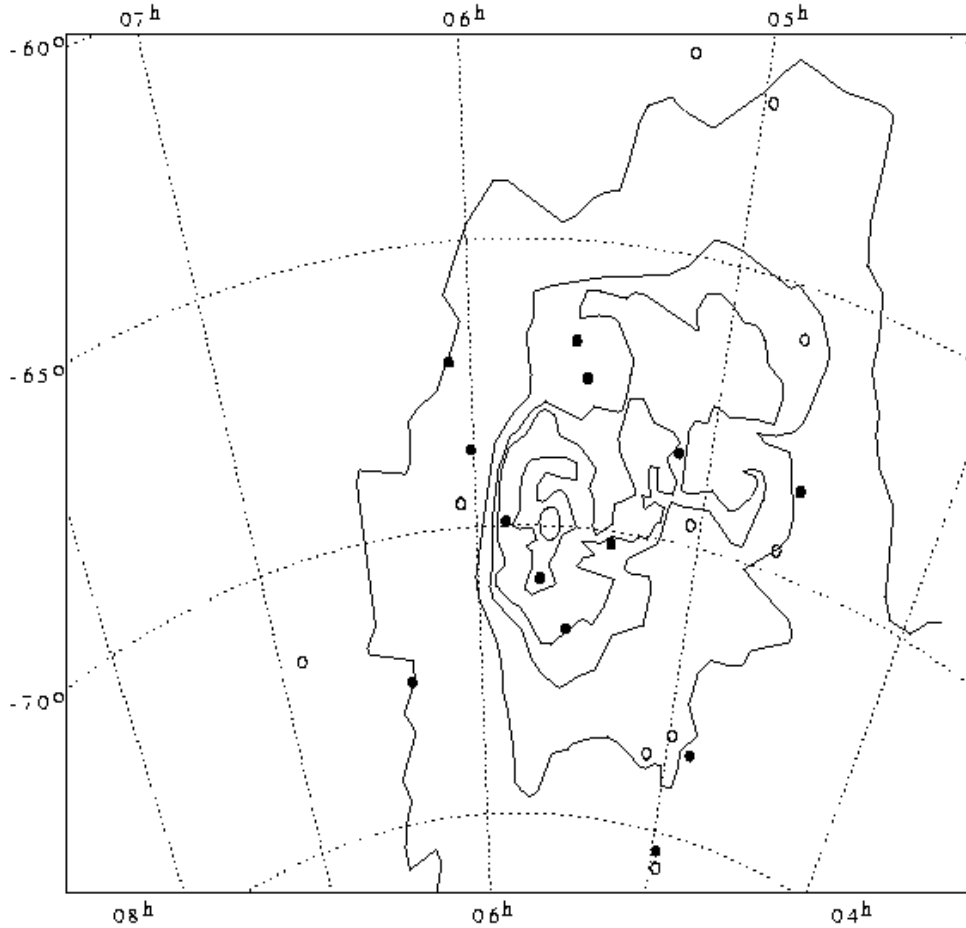


Fig. 2. Angular distribution of the observed LMC background known galaxies (open circles) and candidate galaxies (filled circles). The solid lines represent HI contours of 5, 50, 100, 150, 400 and 600 in units $10^{19} \text{ atoms cm}^{-2}$ from Mathewson & Ford (1984).

vation confirms the latter value (Table 1). The measured velocities were used to bring the galaxy spectra to the rest frame, which is necessary for the subsequent stellar population analysis.

Table 1 shows that the galaxies behind the SMC main body are mostly in the range $10000 < V(\text{km/s}) < 20000$, while those behind the LMC main body are mostly in the range $4000 < V(\text{km/s}) < 6000$. Since we have not a priori selected galaxies differently between the two Clouds the result suggests a real effect, in the sense that towards the LMC a closer galaxy ensemble occurs, which has no counterpart in the SMC background.

Figures 3 and 4 show the resulting rest-frame flux calibrated spectra for the Clouds background galaxies, for which the present study established or confirmed their nature (Sect. 4). Most of these galaxies have red stellar population nuclei, but some are bluer and present features denoting recent star formation such as Balmer absorption

lines (e.g. HS75-20 in the SMC, Fig. 3) or emission lines typical of nuclear H II Regions (e.g. IRAS05538-6645 in the LMC, Fig. 4).

4. Nature of the objects towards the Clouds

We established the nature of the objects towards the Clouds from the radial velocity measurements (Table 1). In the present study velocities resulted either $V > 1000$ km/s or $V < 200$ km/s, undoubtedly characterizing background galaxies and Magellanic Clouds' internal objects, respectively. Most of the objects observed from Hodge & Snow's (1975) list are confirmed as galaxies, except HS75-13 and HS75-18 (upper panel of Fig. 5) which turned out to be a SMC star cluster (H86-159) and a SMC H II region (SMC-N63), respectively (see Sect. 4.1). OHSC3 is confirmed as a LMC star cluster (upper panel of Fig. 5). The objects SMC-DEM92 and HW60 in the SMC,

Table 1. The observed objects towards the Magellanic Clouds.

Object	RA(2000) h:m:s	Dec(2000) °:′:″	l (°)	b (°)	B_t	Exp (sec)	V (km/s)	V_{lit} (km/s)	Type
SMC main body									
HS75-8	00:51:08	-73:39:22	302.96	-43.47		4×900	19650	–	E
AM0054-744sw	00:55:49	-74:30:58	302.53	-42.61		2×900	10685	–	E
SMC-DEM92,AM0054-744ne	00:56:01	-74:30:40	302.52	-42.61		3×900	10369	–	E/S0
HS75-20	00:59:10	-74:02:39	302.20	-43.07		5×900	19017	–	E
HS75-22	01:06:03	-73:59:52	301.55	-43.09		2×900	9890	–	E
HS75-23	01:06:07	-74:07:42	301.56	-42.96		5×900	18950	–	E
HW60	01:09:27	-72:22:21	301.01	-44.69		3×900	17665	–	S
HS75-25,PMNJ0111-7302	01:11:33	-73:02:12	300.89	-44.01		3×900+600	19736	–	E
NGC643B,ESO29G53,IRAS01384-7515	01:39:14	-75:00:41	298.82	-41.73		2×900	4006	3966	
SMC surroundings									
ESO28G12,IRAS00160-7325	00:18:20	-73:09:08	306.24	-43.76	14.90	2×600	6200	6326	S0-a
HS75-10	00:52:34	-70:28:17	302.79	-46.66		3×900	18360	–	E
NGC406,ESO51G18,IRAS01057-7008	01:07:24	-69:52:35	300.91	-47.19	13.02	3×600	1391	1508	Sc
ESO52IG1-NED1	01:24:49	-68:37:21	298.37	-48.21	14.76	2×900	10778	11100	S0-a
NGC802,ESO52G13	01:59:06	-67:52:16	293.50	-48.00	14.09	2×900	1723	1504	SO-a
NGC813,ESO52G16	02:01:37	-68:26:21	293.52	-47.38	13.78	600+420	8188	8160	S0-a
IC5339,ESO77G26,Fairall1051	23:38:05	-68:26:35	312.74	-47.26	14.46	2×900	12250	12328	E-SO
SMC extended objects									
HS75-13,HS6-159	00:55:12	-72:40:57	302.54	-44.44		3×900	180	–	Star cluster
SMC-N63,HS75-18	00:58:17	-72:38:50	302.21	-44.47		2×900	132	–	H II Region
LMC main body									
ESO55G33	04:38:51	-69:30:25	281.49	-36.69	14.39	2×900	5470	–	S0
NGC1669,ESO84G38	04:43:00	-65:48:53	276.96	-37.57	14.78	900+2×600	5580	–	Sa
NGC1809,ESO56G48	05:02:05	-69:34:04	280.76	-34.75	13.19	3×900	1233	1301	Sc
ESO33G11	05:05:07	-73:39:08	285.39	-33.34	14.35	2×900	4550	–	SBaR
NEW GALAXY 1	05:07:38	-68:23:03	279.21	-34.57		2×900+420	5782	–	
HS257,GSC916600034	05:22:45	-70:10:29	280.97	-32.88		2×900	5560	–	
LMC-DEM225,IRAS05319-6723	05:31:49	-67:21:32	277.51	-32.51		3×600	1376	–	
IRAS05338-6645	05:33:52	-66:43:18	276.74	-32.39		3×900	4320	–	
HS356,ESO56G154,KMHK1096,RXJ0534.0-7145	05:33:58	-71:45:20	282.62	-31.70		900+600	7150	7255	
HS394	05:42:02	-70:54:15	281.52	-31.18		3×900	4567	–	
LMC-DEM329,IRAS05522-6952	05:51:42	-69:55:51	280.31	-30.46		2×900	4380	–	
LMC surroundings									
HS17,RXSJ043612.5-682236,HP99-653	04:36:15	-68:22:10	280.27	-37.33		4×900	19250	–	
HS45,IRASF04521-7333	04:51:09	-73:28:42	285.59	-34.33		3×900	7565	–	
ESO33G2	04:55:59	-75:32:28	286.77	-33.29	14.66	2×900	5408	5467	S0
ESO33G3	04:57:47	-73:13:51	285.11	-33.97	14.25	2×600	7664	7677	E
NGC1765,ESO119G24	04:58:24	-62:01:41	271.83	-36.89	13.97	2×900	8846	8758	E
ESO15G18	05:04:58	-81:18:38	293.89	-30.73	14.29	2×900	4926	4903	E
ESO119G48	05:14:36	-61:28:54	270.78	-35.09	13.51	2×900	4549	4548	S0-a
HS449,GH90-060055-6840	06:00:43	-68:40:09	278.81	-29.72		4×900	11305	–	
NGC2187A,ESO57G68sw,AM0604-693sw	06:03:44	-69:35:18	279.86	-29.44	12.94	2×900	3769	3963	Sa
NGC2187B,ESO57G68ne,AM0604-693ne	06:03:52	-69:34:41	279.85	-29.43	13.16	2×900	4519	4470	E
HS451	06:05:28	-67:07:10	277.03	-29.28		3×900	7931	–	
SL887	06:21:01	-72:35:34	283.30	-28.06		3×900+600	11466	–	
ESO58G19	06:52:57	-71:45:44	282.64	-25.55	13.45	2×900	4271	4251	S0-a
LMC extended object									
OHSC3,KMHK362	04:56:36	-75:14:29	287.42	-33.36		4×900	158	–	Star cluster
Comparison B88									
NGC1381	03:36:31	-35:17:39	236.467	-54.039	12.71	2×600	1676	1776	S0
NGC1399	03:38:29	-35:26:58	236.714	-53.636	10.33	2×900	1424	1434	E
NGC1411	03:38:45	-44:06:00	251.02	-52.52	12.18	2×900	1100	1022	E-S0
NGC1404	03:38:52	-35:35:35	236.953	-53.555	10.89	2×600	1970	1926	E
NGC1427	03:42:19	-35:23:37	236.598	-52.854	11.84	2×600	1328	1425	E
NGC1600	04:31:40	-05:05:10	200.416	-33.242	12.04	2×600	4703	4737	E
NGC6758	19:13:52	-56:18:33	340.573	-25.318	12.58	2×600	3489	3408	E
IC4889	19:45:16	-54:20:37	343.538	-29.42	12.02	2×600	2490	2521	E
IC1459	22:57:09	-36:27:37	4.665	-64.106	11.17	2×600	1726	1679	E
South Polar Cap									
NGC148	00:34:16	-31:47:10	340.648	-84.029	13.24	3×600	1705	1516	S0
NGC155	00:34:40	-10:45:59	108.57	-73.169	14.28	5×900	6101	6173	S0
NGC163	00:36:00	-10:07:17	110.121	-72.608	13.92	2×900	5892	5981	E
NGC179	00:37:46	-17:50:56	103.462	-80.2	14.29	2×900	6192	6006	E-S0
NGC277	00:51:17	-08:35:48	122.814	-71.468	14.73	900+600	4120	4327	E-SO
IC1633	01:09:55	-45:55:52	293.099	-70.843	12.55	2×600	7437	7242	E
ESO476G4	01:21:07	-26:43:36	211.145	-83.373	13.86	2×900	5922	5839	E-SOB
ESO352G55	01:21:33	-33:09:23	257.572	-81.133	14.63	2×900	3747	3539	E-SO
ESO542G15	01:27:14	-21:46:24	181.527	-80.258	14.70	2×900	5532	5567	SORing
NGC641	01:38:39	-42:31:40	273.994	-71.847	13.42	2×900	6306	6454	E-SO
NGC720	01:53:00	-13:44:20	173.019	-70.358	11.40	2×600	1563	1736	E
NGC7736	23:42:26	-19:27:09	55.15	-72.418	13.80	4×900	4492	4511	S0
NGC7761	23:51:29	-13:22:53	74.423	-70.37	14.14	3×900	7087	7082	SO

and LMC-DEM225, LMC-DEM329, HS17, HS45, HS257, HS356, HS394, HS449, HS451 and SL887 in the LMC (originally classified as star clusters or H II regions) are shown to be galaxies. In the following we comment on the properties of some objects:

One observed galaxy was not catalogued previously (New Galaxy 1, in Table 1).

HW60 appears to have a companion galaxy (New Galaxy 2, located at J2000 01^h09^m23^s -72°22′15″) at $\approx 0.4'$ to the northwest with dimensions $0.2' \times 0.15'$. They possibly form an interacting system, which is supported by the fact that the HW60's spectrum is blue and presents strong emission lines, suggesting recent star formation

(Fig. 3). Owing to the high radial velocity we do not have the H_{α} , [NII] and [SII] region. Therefore, some nuclear activity cannot be ruled out.

SMC-DEM92 is the brighter member of the interacting pair AM0054-744 (Arp & Madore 1987). We also observed the companion AM0054-744sw (Table 1, Fig. 3). Their radial velocities (Table 1) are comparable, supporting an interaction. A similar case is the interacting pair NGC2187A and NGC2187B (Table 1), which is also an entry in Arp & Madore's catalogue.

In the SMC background the galaxy HS75-25 is an X-ray emitter (Haberl et al. 2000), see present Table 1 for coordinates and other designation. Behind the LMC are

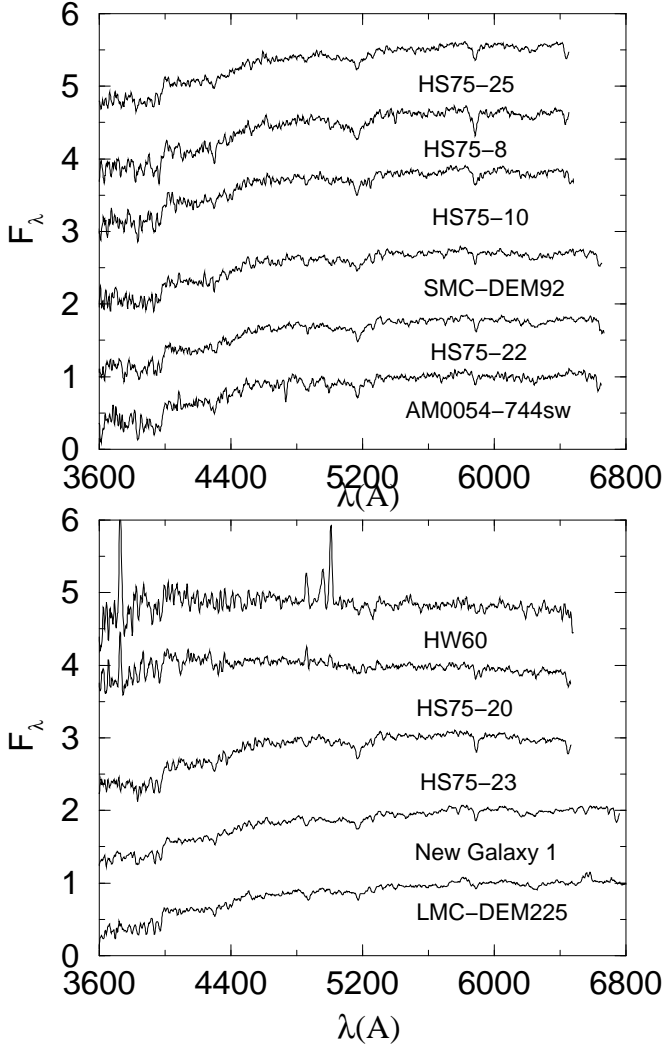


Fig. 3. Rest-frame spectra of objects which turned out to be or were confirmed as SMC background galaxies, together with two LMC's (New Galaxy 1 and LMC-DEM225)

X-ray emitters corresponding to HS17, HS257 (Haberl & Pietsch 1999) and HS356 (Crampton et al. 1997). In particular, HS356 in a rich LMC field has been catalogued not only as star cluster (Hodge & Sexton 1966, Kontizas et al. 1990) but as a galaxy as well (Lauberts 1982).

ESO52IG1 (Lauberts 1982) refers to a compact group of galaxies, studied by Sérsic (1974) – Se10/2, and Arp & Madore (1987) – AM0123-685. The present galaxy is the brightest member of the group (accurate coordinates in Table 1). We point out that the literature coordinates often refer to the group centre. The NED database currently lists the 3 brighter members, but all coordinates are systematically shifted $\approx 0.7'$ to the northeast.

Some galaxies behind the Clouds are IRAS sources (Table 1).

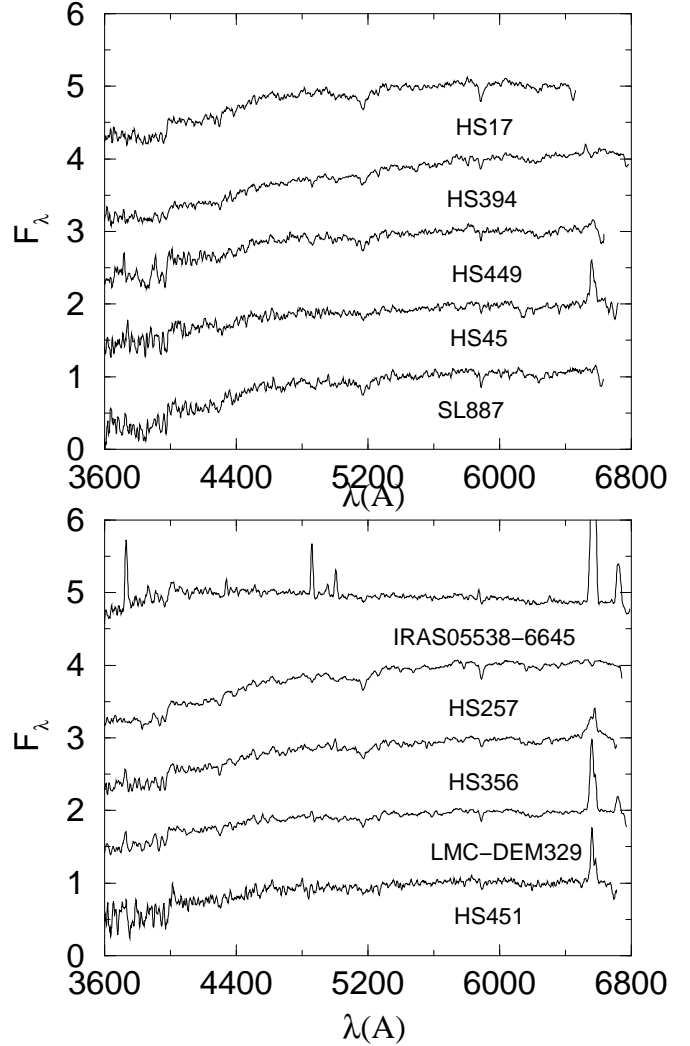


Fig. 4. Same as Fig.3 for LMC background galaxies.

4.1. Discussion of the LMC and SMC extended objects

Bica & Schmitt (1995) and Bica & Dutra (2000) indicated that the object SMC-N63 (Henize 1956) is also present in several other emission object catalogues as L61-331 (Lindsay 1961), SMC-DEM94 (Davies et al. 1976) and MA1065 (Meyssonier & Azzopardi 1993). The present cross-identification of this object with HS75-18 together with its CCD spectrum (upper panel of Fig. 5) conclusively establishes its nature as an H II region. The stellar content of the H II region was catalogued as the star cluster SMC-OGLE113 (Pietrzyński et al. 1998). The gas reddening including the foreground reddening can be derived from the emission line spectrum (upper panel of Fig. 5) using the Balmer decrement $F_{H\alpha}/F_{H\beta} = 3.31$. Assuming case B of the recombination-line theory the intrinsic ratio is $(F_{H\alpha}/F_{H\beta})_0 = 2.87$ (Osterbrock 1989), wherefrom we derive $E(B-V) = 0.13$. This value is lower than SFD98's dust emission reddening estimate $E(B-V)_{FIR} = 0.37$. A

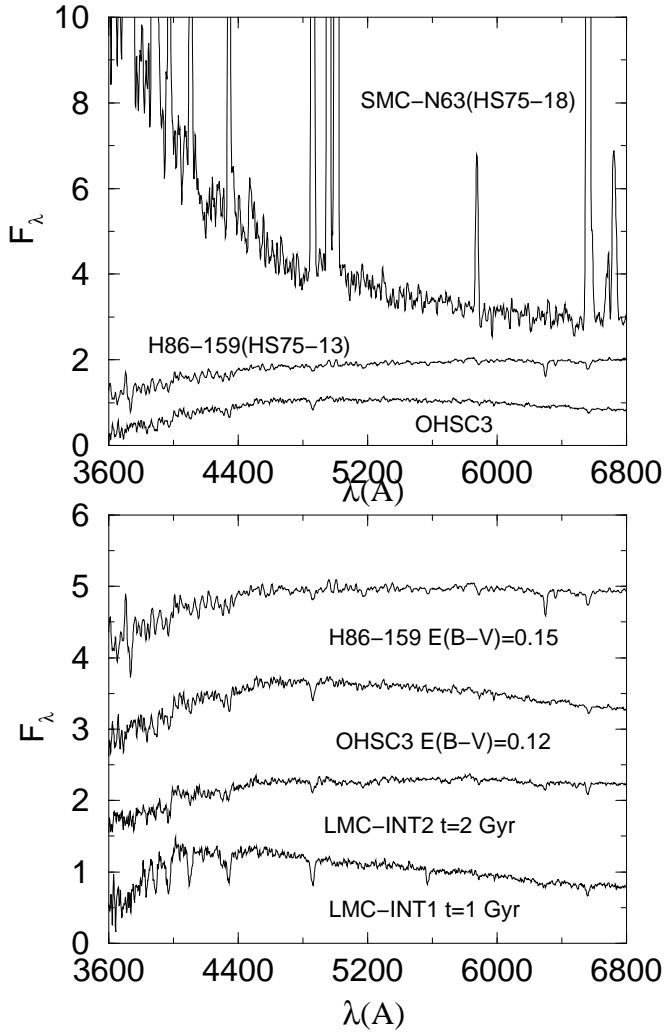


Fig. 5. Upper panel: Objects which turned out to be or were confirmed as extended objects belonging to the SMC (H II Region HS75-18 and star cluster HS75-13), and LMC (star cluster OHSC3). Lower panel: age and reddening estimates using LMC cluster templates

possible explanation for this difference is that the molecular cloud related to this recent star forming region is located behind SMC-N63.

Integrated spectra of star clusters as compared to template cluster spectra of different ages and metallicities can provide parameters such as age and reddening (e.g. Piatti et al. 1998, Ahumada et al. 2000). In the present study the signal-to-noise ratios of the H86-159 and OHSC3 spectra are not ideal for a detailed study of the cluster spectral features, but the spectral distribution can be compared to templates (lower panel of Fig. 5).

Using a deep plate from the CTIO 4-meter telescope Hodge (1986) catalogued the star cluster H86-159, and CCD images confirmed that (SMC-OGLE102 – Pietrzyński et al. 1998). The present study cross-identifies the latter object with HS75-13 and its spectrum (upper

panel Fig. 5) confirms that one is not dealing with a galaxy. Recently de Oliveira et al. (2000) estimated a total reddening $E(B-V)_{MW+SMC} = 0.10$ and age ≈ 500 Myr for H86-159 from a colour-magnitude diagram (CMD) extracted from the OGLE photometric database (Udalski et al. 1998). As comparison (lower panel of Fig. 5) we show the reddening-free LMC cluster templates LMC-Int1 and LMC-Int2, respectively of ages 1 and 2 Gyr (Dutra et al. 1999). By applying reddening corrections to the spectrum of H86-159 following Seaton’s (1979) extinction law, we derive $E(B-V)_{MW+SMC} = 0.15$ and an age of 2 Gyr. In the cluster direction SFD98’s dust emission reddening is $E(B-V)_{FIR} = 0.38$. The object is central in the SMC and star forming regions are nearby (traces of diffuse gas are denoted by [OII] $\lambda 3727$ Å, [OIII] $\lambda\lambda 4959, 5007$ Å superimposed on the cluster spectrum), so that important dust emission is expected in the area. The high dust emission reddening as compared to the stellar content methods (CMD and spectrum) suggests the presence of dust in the cluster background within the SMC, similarly to star cluster directions in the Galaxy (Dutra & Bica 2000). In contrast to background galaxies, Cloud clusters do not necessarily probe the total internal dust column of the Magellanic Clouds themselves. The age difference for the cluster can be explained by the fact that it is a poorly populated cluster. The turnoff is close to the photometric limit and the field is rich, which can affect significantly the CMD age determination. On the other hand, stochastic effects for bright stars and field contamination for such low mass clusters may cause important uncertainties on the integrated properties (e.g. Geisler et al. 1997). At any rate the bracket 0.5 - 2 Gyr is a considerable constraint on the cluster age.

OHSC3 (Olszewski et al. 1988) or KMHK362 (Kontizas et al. 1990) was catalogued as a star cluster. It called our attention owing to the compact nature in ESO/SERC sky survey plates. There is a neighbouring galaxy $\approx 2.3'$ to the northeast. This galaxy (New Galaxy 3) is an inclined spiral with dimensions $\approx 0.6' \times 0.2'$ located at J2000 $04^h 57^m 05^s -75^\circ 13' 08''$. We suspected a galaxy pair, but this is not confirmed by the OHSC3 spectrum. In this direction SFD98 predict $E(B-V)_{FIR} = 0.12$, which was applied in the reddening correction of the OHSC3 spectrum (lower panel of Fig. 5). The spectral properties appear to be intermediate between the two template spectra leading to an age ≈ 1.5 Gyr.

5. Reddening-free galaxy templates

Red stellar population galaxy nuclei are ideal as reddening probes since the spectral distribution is essentially insensitive to age variations of the components, and present a small dependence on metallicity (B88). Blue stellar populations have stronger continuum variations with age distribution of the components.

B88 studied the stellar populations of early and late type galaxies by means of their nuclear integrated spectra. Early and late type galaxy nuclei were studied separately considering also luminosity differences (B88 and references therein). Spectra with similar equivalent widths and dereddened continuum distribution were grouped into high signal-to-noise templates. These templates represent the most frequent types of stellar populations found in normal galaxy nuclei. The early type templates E1 to E3 represent a decreasing metallicity sequence among giant early type galaxy nuclei dominated by old (red) stellar populations. E7 represents nuclei dominated by old populations but with significant contribution of 0.5 to 1 Gyr components. S1 to S3 represent a similar metallicity sequence to E1-E3 for red stellar populations occurring in giant spiral galaxy nuclei. Finally, S4 to S7 is a sequence of giant spiral galaxy nuclei with increasing contributions of young stellar populations.

For the spectral comparisons between sample galaxies and templates we employ equivalent widths (W) of strong absorption features. We use as metal features K CaII, CN, G Band, MgI and NaI, together with four Balmer lines. In Table 2 are shown W values for templates and individual galaxies measured with continuum tracings and feature windows following Bica & Alloin (1986) and Bica et al. (1994). For bluer stellar populations we increased the resolution of spectral properties by creating the intermediate templates S5/S6 ($0.5 \times S5 + 0.5 \times S6$), S6/S7A ($0.5 \times S6 + 0.5 \times S7$) and S6/S7B ($0.25 \times S6 + 0.75 \times S7$). This procedure in turn provides a higher resolution in reddening determinations since the continuum varies strongly for increasing contents of younger populations in galaxy nuclei. Typical W errors are $\approx 5\%$ and depend mostly on signal-to-noise ratio and uncertainties in the continuum positioning.

Red stellar populations are the most frequent types in the background samples (Figs. 3 and 4). In addition to the high reddening accuracy that they can provide (Sect. 6), it is important also to minimize possible observational uncertainties by creating templates from galaxies observed in the same observing runs. For these purposes we built new red stellar population templates using South Polar Cap galaxies (Sect. 2.2) and some galaxies in common with B88, which have $E(B-V)_{FIR} < 0.02$ (Table 3) to avoid dust cirrus (Sect. 2.2). Measurements of W s for these galaxies (Table 2) allowed us to classify them into types E1, E2 or E3. We dereddened the spectra using $E(B-V)_{FIR}$ values and Seaton's (1979) galactic extinction law. At this stage, the E2 and E3 member galaxies turned out to be very similar in terms of continuum distribution. Therefore we adopted two reference spectra T1 and T23 as counterparts in the present study of the E1 and E2/E3 templates. Members of T1 and T23 are indicated in Table 3. The remaining galaxies with somewhat higher reddening values (Table 3) have either internal reddening as dusty ellipticals (Ferrari et al. 1999) and/or foreground contribution.

It is possible to determine a spectroscopic reddening value $E(B-V)$ by fitting the observed galaxy spectrum to that of the corresponding template with similar W s and applying continuum corrections according to Seaton's law. We provide in column 4 of Table 3 results for individual galaxies in the templates T1 and T23 themselves and additional red stellar population galaxies in the same regions.

Table 3 indicates that dust emission and spectroscopic reddening values are consistent for small amounts of reddening. The average of spectroscopic reddening values in the present South Polar Cap sample (13 galaxies) is $E(B-V) = 0.02 \pm 0.01$, which is consistent with SFD98's estimate (Sect. 2.2).

6. Reddening towards the Magellanic Clouds

For each background galaxy we searched for the template spectrum with comparable W s (Table 2) which was assumed as the reddening-free reference stellar population. The resulting templates are shown in column 2 of Table 4. Making use of Seaton's law and varying the reddening amount we dereddened the observed galaxy spectrum to match the template continuum distribution. The upper panel of Figure 6 illustrates the reddening determination for a red stellar population galaxy (HS394). Note the important reddening effect in the observed spectrum. The lower panel illustrates a blue stellar population nucleus (IRAS05338-6645). The reddening values obtained by this spectroscopic procedure are given in column 3 of Table 4. For comparison purposes the dust emission reddening $E(B-V)_{FIR}$ value is shown in column 4. Finally, in column 5 we give the HI column density in units of 10^{19} atoms cm^{-2} (Mathewson & Ford 1984).

The uncertainties in the matching of the continuum distributions is small $\epsilon E(B-V) \approx 0.01$. The largest source of uncertainties arises from the determination of the stellar population. For red stellar populations this uncertainty is typically $\epsilon E(B-V) \approx 0.02$, and somewhat larger for blue stellar populations ($\epsilon E(B-V) \approx 0.05$).

Out of 36 SMC and LMC background galaxies, 31 show good agreement ($\delta E(B-V) \leq 0.10$) between the spectroscopic and dust emission reddening values (Table 4), leading to a r.m.s. of differences of 0.04. One case of significant difference (HS75-8) is behind the SMC main body, and the remaining ones (New Galaxy 1, HS356, HS394 and LMC-DEM329) behind the LMC main body. In the latter 5 cases $E(B-V)_{FIR}$ is larger and HI column densities are important (Table 4). Since the slit apertures are typically $4'' \times 8-10''$ (Sect. 3) and SFD98's pixel dimensions $142'' \times 142''$, a possible explanation is that the dust distribution is patchy with a scale significant smaller than SFD98's pixel. We note that out of the five galaxies with significant differences three have red stellar populations (Table 4) and the spectroscopic reddening values are accurate.

The largest difference occurs for New Galaxy 1 which has a very high reddening value $E(B-V)_{FIR} = 0.68$ (Ta-

Table 2. Ws for strong absorption features in the template and individual galaxy spectra

Object	K	H δ	CN	G	H γ	H β	MgI	NaI	H α
Windows	3908-3952	4082-4124	4150-4214	4284-4318	4318-4364	4846-4884	5156-5196	5880-5914	6540-6586
B88 Templates									
E1	17.5	5.7	15.1	9.6	5.2	3.7	10.9	6.6	0.2
E2	17.9	5.8	12.1	9.6	5.7	3.5	9.6	5.4	1.6
E3	16.1	2.3	7.9	8.9	4.3	4.2	8.0	4.2	2.2
E7	12.3	6.1	6.9	6.9	5.4	4.9	7.4	4.1	---
S4	13.2	4.7	5.8	7.3	5.0	3.5	6.1	4.1	e
S5	7.7	3.9	5.5	6.3	3.3	0.9	6.1	4.1	e
S5/S6	6.1	4.1	4.0	5.5	3.5	0.0	5.3	3.7	e
S6	5.6	4.2	2.6	4.7	3.6	e	4.0	3.4	e
S6/S7A	2.5	4.7	2.0	3.5	3.6	e	3.7	3.2	e
S6/S7B	3.1	4.9	2.0	3.3	4.0	e	3.8	3.3	e
S7	2.9	5.4	2.3	3.1	4.1	e	3.9	3.5	e
New Red Population Templates									
T1	18.6	6.1	15.0	9.6	4.3	3.4	11.3	7.0	0.2
T23	17.1	4.3	10.2	9.2	4.4	3.5	8.7	4.3	0.8
Comparison (B88)									
NGC1381	18.4	3.6	10.0	8.7	4.4	4.0	8.2	4.2	1.9
NGC1399	19.4	7.5	16.7	8.6	4.3	4.1	12.6	7.5	1.6
NGC1411	16.7	4.3	10.6	9.4	4.3	3.2	8.4	4.7	---
NGC1404	18.7	7.2	12.7	11.0	4.4	3.4	10.1	6.7	2.3
NGC1427	19.0	5.5	11.8	9.8	6.4	4.1	9.5	4.5	1.1
NGC1600	18.5	6.4	15.5	8.9	4.3	4.1	12.1	5.8	2.2
NGC6758	18.7	8.6	15.3	10.7	5.6	4.2	10.1	6.1	1.4
IC4889	20.1	9.2	12.6	11.9	8.2	2.9	7.1	2.9	---
IC1459	20.4	5.4	13.8	9.0	3.6	2.0	11.2	6.9	---
South Polar Cap									
NGC148	19.4	7.6	12.2	10.5	5.4	4.3	9.2	6.1	2.9
NGC155	17.3	4.8	10.7	10.7	6.1	5.4	9.5	4.2	---
NGC163	17.2	4.9	13.5	9.1	5.2	2.8	9.8	5.0	1.3
NGC179	16.8	6.9	12.1	9.7	5.5	4.4	8.4	4.0	---
NGC277	17.9	6.4	13.3	10.7	6.1	4.0	10.1	5.2	---
IC1633	18.6	4.9	9.3	9.8	7.1	2.9	8.0	4.7	---
ESO476G4	16.2	2.4	8.0	9.3	3.5	2.7	8.0	3.8	2.0
ESO352G55	19.6	5.8	11.8	8.9	4.9	3.9	9.5	5.4	2.3
ESO542G15	17.0	4.3	9.5	8.8	5.1	3.9	8.2	4.1	1.6
NGC641	17.3	5.2	11.4	9.3	3.9	3.2	9.4	4.0	---
NGC720	18.7	7.1	15.3	9.4	4.9	2.2	10.9	6.9	---
NGC7736	19.0	6.5	13.8	9.7	6.1	4.8	10.3	5.6	2.2
NGC7761	13.6	5.7	10.0	8.9	6.4	4.5	8.4	3.2	---
SMC Main body									
HS75-8	17.2	4.9	13.5	9.1	5.2	2.8	9.8	5.0	1.3
AM0054-744sw	20.4	1.7	6.7	9.2	3.9	5.1	8.5	4.1	2.3
SMC-DEM92	16.7	1.3	9.2	8.1	5.9	3.6	6.9	3.6	1.8
HS75-20	4.7	6.3	2.3	4.4	5.6	e	5.5	4.3	---
HS75-22	16.5	4.5	12.9	8.8	5.1	2.4	8.9	4.5	1.0
HS75-23	15.2	---	6.9	8.5	4.6	3.3	10.0	5.7	---
HS75-25	18.6	4.9	9.3	9.8	7.1	2.9	8.0	4.7	---
NGC643B	7.9	8.4	4.6	4.9	7.6	2.9	3.7	2.4	e
SMC surroundings									
ESO28G12	6.5	4.8	2.9	6.3	3.9	e	4.7	3.2	e
HS75-10	19.8	3.9	14.0	9.0	6.4	2.9	8.7	5.9	2.4
NGC406	9.8	5.0	2.3	4.1	5.7	e	3.3	1.7	e
ESO521G1-NED1	18.5	4.9	13.3	9.1	4.8	4.0	9.5	5.1	2.6
NGC802	0.7	6.0	1.5	2.5	5.0	e	2.3	2.1	e
NGC813	14.3	3.7	8.7	8.8	5.2	3.5	6.8	3.1	2.8
IC5339	16.7	2.9	7.9	8.4	3.9	3.8	9.9	6.2	---
LMC									
LMC Main body									
ESO55G33	11.4	5.0	8.1	7.3	5.7	1.3	6.1	3.2	e
NGC1669	5.6	5.2	2.5	4.7	3.5	2.3	6.0	2.8	e
NGC1809	5.2	9.3	3.7	3.1	5.8	1.7	3.0	2.8	e
ESO33G11	17.4	4.2	11.0	9.0	5.0	2.7	7.6	3.1	e
NEW GALAXY 1	14.9	5.8	10.3	8.5	5.7	3.5	7.8	4.6	2.3
HS257	20.2	6.4	13.3	9.8	4.6	3.5	10.0	5.5	1.9
LMC-DEM225	12.1	4.2	6.2	6.8	5.0	4.3	5.7	3.6	---
IRAS05338-6645	4.9	4.6	3.5	3.6	1.4	e	3.0	2.0	e
HS356	14.2	5.0	8.9	7.9	4.3	1.9	7.2	3.0	e
HS394	16.6	3.4	8.1	9.7	5.5	4.1	8.2	3.4	1.3
LMC-DEM329	8.0	4.4	6.4	5.8	3.0	e	5.5	2.8	e
LMC surroundings									
HS17	16.2	5.1	12.4	8.5	3.6	2.1	10.0	6.6	---
HS45	10.7	6.8	5.1	7.3	7.8	2.8	5.3	2.5	e
ESO33G2	14.0	3.4	9.5	8.0	3.4	e	6.3	3.5	e
ESO33G3	18.0	7.6	13.14	9.9	4.1	3.6	8.5	3.9	---
NGC1765	19.2	6.2	14.7	9.7	5.0	3.1	9.8	6.0	1.5
ESO15G18	16.7	2.1	10.2	8.9	4.8	2.9	7.8	4.6	e
ESO119G48	15.4	3.3	9.6	8.3	4.3	3.6	7.8	4.3	1.4
HS449	13.5	4.0	8.4	7.7	6.4	4.0	7.8	3.8	e
NGC2187A	18.6	4.5	13.6	10.0	5.1	3.7	10.0	5.6	2.3
HS451	8.9	3.5	6.9	6.4	4.3	2.6	4.3	2.8	e
SL887	17.2	6.0	13.3	9.1	3.7	4.9	8.1	4.7	---
ESO58G19	15.7	3.0	11.9	10.3	5.1	3.0	8.4	4.5	1.4

Note: e - indicates Balmer line in emission.

ble 4). This galaxy is projected at the edge of the shell emission nebula LMC-DEM76 (Davies et al. 1976). An alternative explanation to dust small scale variations is that dust in this region may be heated beyond the temperature correction range employed by SFD98. Evidence of a similar effect was pointed out by Dutra & Bica (2000) for the Galactic Center direction.

The galaxy LMC-DEM225 (Fig. 3) has a rare stellar population type dominated by a red stellar population,

but with an important Balmer-line in absorption component in the range 3700 Å to 3900 Å. The most similar template in terms of Ws available in B88 is E7 (Table 2). The enhanced Balmer lines in the violet region might be explained by a somewhat younger burst (100 - 500 Myr) in LMC-DEM225, rather than the 1 Gyr burst in E7 (B88). Owing to the stellar population difference we have not determined reddening for this galaxy.

Table 3. Spectroscopic and dust emission reddening values for observed galaxies in the B88 and South Polar Cap samples.

		Comparison galaxies from B88		
Object	Template	comments	E(B-V)	E(B-V) _{FIR}
NGC1381	T23	member	0.01	0.01
NGC1399	T1	member	0.01	0.01
NGC1411	T23	member	0.01	0.01
NGC1404	T1	member	0.02	0.01
NGC1427	T23	member	0.01	0.01
NGC1600	T1	dusty	0.02	0.04
NGC6758	T1	dusty	0.05	0.07
IC4889	T23	dusty	0.05	0.05
IC1459	T1	member	0.03	0.02
		South Polar Cap		
Object	Template	Comments	E(B-V)	E(B-V) _{FIR}
NGC148	T23	member	0.02	0.02
NGC155	T23		0.02	0.03
NGC163	T1		0.01	0.03
NGC179	T23	member	0.02	0.02
NGC277	T1		0.01	0.04
IC1633	T23	member	0.02	0.01
ESO476G4	T23	member	0.01	0.01
ESO352G55	T23		0.05	0.03
ESO542G15	T23	member	0.01	0.02
NGC641	T23	member	0.02	0.02
NGC720	T1	member	0.01	0.02
NGC7736	T1		0.03	0.03
NGC7761	T23		0.03	0.03

The galaxies projected on SMC surroundings (HI column density $<50 \times 10^{19}$ atoms cm^{-2}) have an average spectroscopic reddening value of $E(B-V) = 0.01 \pm 0.02$. This value is comparable to that of the South Polar Cap galaxies (Sect. 5), showing that at least in the direction of the SMC no significant difference occurs between the Polar region and $b \approx -45^\circ$. This value is also comparable to the average dust emission reddening in the SMC surroundings $E(B-V)_{FIR} = 0.03 \pm 0.01$ (Table 4) and that derived by SFD98 in the same region (Sect. 1). Considering the galaxies behind the SMC main body the average spectroscopic reddening is $E(B-V) = 0.05 \pm 0.05$ and that from dust emission in the corresponding lines of sight is $E(B-V)_{FIR} = 0.07 \pm 0.04$. By subtracting the average of reddening values in the main body directions from those in the surroundings, both the spectroscopic and dust emission methods predict an internal SMC reddening $\Delta E(B-V) = 0.04$ which is consistent with the fact that important HI column density differences occur between these regions (Table 4).

In the LMC surroundings (HI density column $<50 \times 10^{19}$ atoms cm^{-2}) the average spectroscopic reddening is $E(B-V) = 0.06 \pm 0.03$ which is similar to the average dust emission reddening value in the corresponding directions $E(B-V)_{FIR} = 0.08 \pm 0.04$ (Table 4). These values are in turn similar to those derived by SFD98 (Sect. 1). We conclude that in the LMC direction at $b \approx -33^\circ$ the Milky Way reddening becomes evident as compared to the Polar

Cap. For the LMC main body the average spectroscopic reddening is $E(B-V) = 0.12 \pm 0.10$. Considering only the red population galaxies, which provide the most accurate determinations, the result is basically the same $E(B-V) = 0.15 \pm 0.11$. This suggests an intrinsic dispersion among lines of sight. We estimate $\Delta E(B-V) = 0.06$ between LMC main body directions and surroundings.

7. Concluding remarks

Spectra of nuclear regions of galaxies towards the Magellanic Clouds are useful reddening probes in the Milky Way and the Clouds themselves. By means of radial velocities we established the nature of ≈ 20 objects in terms of background galaxies or star clusters and H II regions belonging to the Clouds. The radial velocities of the observed galaxies behind the Magellanic Clouds reveal an interesting spatial distribution: most of the brighter galaxies in the main body of the LMC are in the range $4000 < V(\text{km/s}) < 6000$, while for the SMC they are more distant in the range $10000 < V(\text{km/s}) < 20000$.

We estimated reddening values by comparing observed galaxy spectra with reddening-free templates of similar stellar populations. We inferred the reddening distribution throughout the Clouds by means of 18 galaxies in the main bodies and 18 in the surroundings. The SMC foreground reddening ($E(B-V)_{MW} = 0.01$) is comparable to that of the South Polar Cap, while that of the LMC,

Table 4. Spectral and dust emission reddening values for galaxies towards the Magellanic Clouds.

SMC				
Object	Template	E(B-V)	E(B-V) _{FIR}	HI column
Main body				
HS75-8	T1	0.03	0.15	675
AM0054-744sw	T23	0.00	0.05	136
SMC-DEM92	T23	0.00	0.05	130
HS75-20	S6/S7B	0.10	0.05	210
HS75-22	T23	0.04	0.04	140
HS75-23	T23	0.00	0.04	123
HS75-25	T23	0.10	0.10	484
NGC643B	S6	0.12	0.05	82
surroundings				
ESO28G12	S6	0.00	0.04	37
HS75-10	T1	0.01	0.02	27
NGC406	S6/S7A	0.00	0.02	18
ESO52IG1-NED1	T23	0.04	0.03	20
NGC802	S7	0.00	0.02	28
IC5339	T23	0.01	0.04	outside
LMC				
Object	Template	E(B-V)	E(B-V) _{FIR}	HI column
Main body				
ESO55G33	S5	0.10	0.15	50
NGC1669	S6	0.10	0.05	75
NGC1809	S7	0.23	0.24	75
ESO33G11	T23	0.09	0.13	55
NEW GALAXY 1	T23	0.04	0.68	136
HS257	T23	0.15	0.24	141
IRAS05538-6645	S7	0.20	0.13	87
HS356	S4	0.00	0.13	158
HS394	T23	0.32	0.50	446
LMC-DEM329	S56	0.02	0.22	186
surroundings				
HS17	T23	0.06	0.06	40
HS45	S5	0.02	0.12	44
ESO33G2	S4	0.08	0.13	outside
ESO33G3	T1	0.09	0.11	outside
NGC1765	T1	0.03	0.03	7
ESO15G18	T23	0.10	0.10	outside
ESO119G48	T23	0.01	0.02	outside
HS449	T23	0.01	0.06	25
NGC2187A	T1	0.07	0.10	27
HS451	S6	0.05	0.07	5
SL887	T23	0.07	0.08	outside
ESO58G19	T23	0.10	0.11	outside

at a lower galactic latitude is higher ($E(B-V)_{MW} = 0.06$). Both Clouds are quite transparent, at least in the sampled lines of sight. The derived average internal reddening values are $E(B-V)_i = 0.04$ and 0.06 , respectively for the SMC and LMC. The resulting statistics on reddening values are likely to be skewed toward lower reddening values, since heavily reddened galaxies are less likely to be detected, especially in the most crowded central regions in the Clouds.

Following the reddening study in the Milky Way by Dutra & Bica (2000), which analyses reddening values de-

rived from dust emission and stellar content of star clusters, the present method probes the foreground and internal reddening in the Clouds by means of background galaxies. We conclude that the dust emission and stellar population reddening values towards the Clouds agree well for 86 % of the present sample. The significant differences found are in the sense of larger $E(B-V)_{FIR}$ values. Possible explanations are patchy dust distribution in a scale smaller than SFD98's resolution or dust heated above the range of the temperature map.

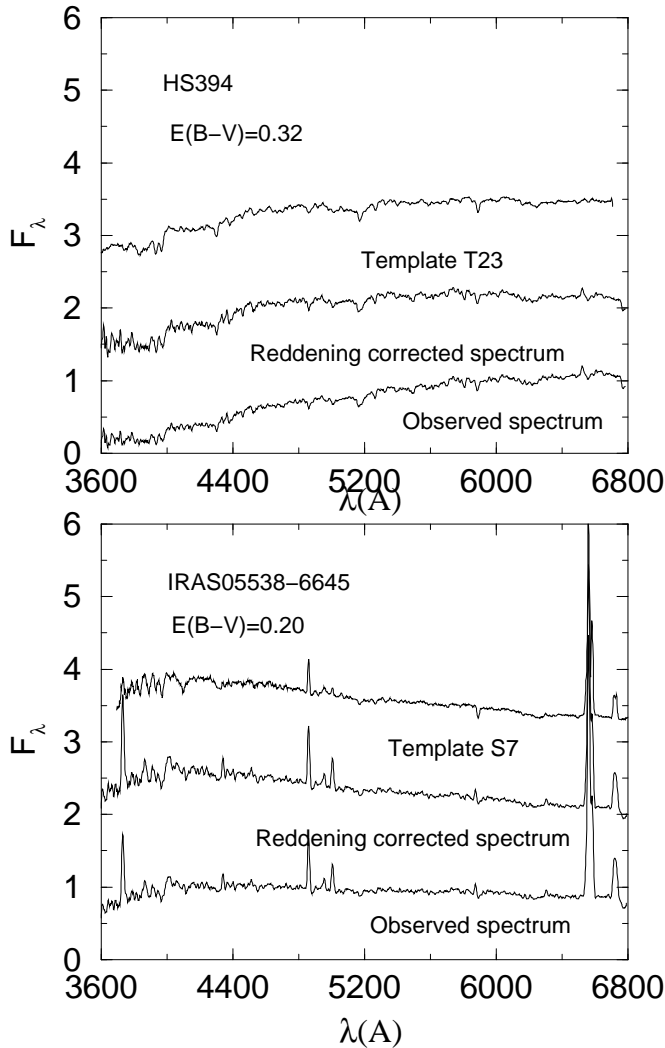


Fig. 6. Upper panel: Example of reddening determination for a red stellar population nucleus. Lower panel: Example of reddening determination for a blue stellar population nucleus.

In order to map out in detail the dust distribution in the Magellanic Clouds large samples of background galaxies are necessary. We note that several of the present main body galaxies are not obvious on Sky Survey images, because of crowding and proximity to extended objects in the Clouds. A fundamental question is whether more reddened zones exist in the Clouds, especially in the LMC. It would be important to carry out higher resolution imaging to identify galaxies for spectroscopy in large telescopes.

Acknowledgments

We thank the CASLEO staff for hospitality and support during the observing runs. The authors acknowledge use of the CCD and data acquisition system supported under U.S. National Science Foundation grant AST-90-15827 to R.M. Rich. We have made use of the LEDA database,

(<http://leda.univ-lyon1.fr>), and the NASA/IPAC Extragalactic Database (NED) which is operated by the Jet Propulsion Laboratory, California Institute of Technology, under contract with the National Aeronautics and Space Administration. We use images from the Digitized Sky Survey (produced at the Space Telescope Science Institute under U.S. Government grant NAG W-2166) by means of the Canadian Astronomy Data Centre (CADC) interface. This work was partially supported by the Brazilian institutions CNPq and FINEP, the Argentine institutions CONICET, ANPCyT and SECYT (UNC), and the VI-TAE and Antorchas foundations.

References

- Ahumada A.V., Clariá J.J., Bica E., Piatti A.E. 2000, *A&AS*, 141, 79
- Arp H.C., Madore B.F. 1987, *in A Catalogue of Southern Peculiar Galaxies and Associations*, Cambridge Univ. Press
- Baldwin J.A., Stone R.P.S. 1984, *MNRAS*, 206, 241
- Bica E. 1988, *A&A*, 195, 76
- Bica E., Alloin D. 1986, *A&A*, 162, 21
- Bica E., Alloin D., Schmitt H. 1994, *A&A*, 283, 805
- Bica E., Schmitt H.R. 1995, *ApJS*, 54, 33
- Bica E., Schmitt H.R., Dutra C.M., Luz Oliveira H. 1999, *AJ*, 117, 238
- Bica E., Dutra C.M. 2000, *AJ*, 119, 1214
- Burstein D., Heiles C. 1978, *ApJ*, 225, 40
- Burstein D., Heiles C. 1982, *AJ*, 87, 1165
- Crampton D., Gussie G., Cowley A.P., Schmidtke P.C. 1997, *AJ*, 114, 2353
- Davies R.D., Elliot K.H., Meaburn J. 1976, *Mmras*, 81, 89
- de Oliveira M., Dutra C.M., Bica E., Dottori H. 2000, *A&AS*, 146, 57
- de Vaucouleurs G., de Vaucouleurs A., Corwin H.G. 1976 *in Second Reference Catalogue of Bright Galaxies*, University of Texas Press (RC2)
- Dutra C.M., Bica E., Clariá J.J., Piatti A.E. 1998, *in The formation and evolution of galaxies* Bol. Acad. de Ciencias de Córdoba, 62, p.127
- Dutra C.M., Bica E., Clariá J.J., Piatti A.E. 1999, *MNRAS*, 305, 373
- Dutra C.M., Bica E. 2000, *A&A*, 359, 347
- Ferrari F., Pastoriza M.G., Macchetto F., Caon N. 1999, *A&AS*, 136, 269
- Geisler D., Bica E., Dottori H., Clariá J.J., Piatti A.E., Santos, J.F.C. Jr. 1997, *AJ*, 114, 1920
- Gurwell M., Hodge P. 1990, *PASP*, 102, 849
- Haberl F., Pietsch W. 1999, *A&AS*, 139, 277
- Haberl F., Filipovic M.D., Pietsch W., Kahabka P. 2000, *A&AS*, 142, 41
- Henize K.G. 1956, *ApJS*, 2, 315
- Hodge P.W., Sexton J.A. 1966, *AJ*, 71, 363
- Hodge P.W. 1974, *ApJ*, 192, 21
- Hodge P.W., Wright F.W. 1974, *AJ*, 79, 858
- Hodge P.W., Snow T.P. 1975, *AJ*, 80, 9
- Kontizas M., Morgan D.H., Hatzidimitriou D., Kontizas E. 1990, *A&AS*, 84, 527
- Lauberts A., 1982 *The ESO/Uppsala Survey of the ESO (B) Atlas*, European Southern Observatory, Garching bei München

- Lindsay E.M. 1961, AJ, 66, 169
MacGillivray H.T. 1975, MNRAS, 170, 241
Mathewson D.S., Ford V.L. 1984, IAU Symp. No 108, 125
Meyssonnier N., Azzopardi M. 1993, A&AS, 102, 451
Oestreicher M.O., et al. 1995, A&AS, 112, 495
Oestreicher M.O., Schmidt-Kaler Th. 1996, A&AS, 117, 303
Olszewski E.W., Harris H.C., Schommer R.A., Canterna R.W.
1988, AJ, 95, 84
Osterbrock D.E. 1989, *in Astrophysics of Gaseous Nebulae*,
Univ. Science Books, Mill Valley, California
Piatti A.E., Bica E., Clariá J.J. 1998, A&AS, 127, 423
Pietrzyński G., Udalski A., Szymański M., et al. 1998, Acta
Astron., 48, 175
Pietrzyński G., Udalski A. 1999, Acta Astron., 49, 157
Reach W.T., Wall W.F., Odegard N. 1998, ApJ, 507, 507
Sandage A. 1973, ApJ, 183, 711
Schlegel D.J., Finkbeiner D.P., Davis M. 1998, ApJ, 500, 525
Seaton M.J. 1979, MNRAS, 187, 73p
Sérsic J.L. 1974, ApSS, 28, 365
Shapley H., Lindsay E.M. 1963, Irish AJ, 6, 74
Udalski A., Szymański M., Kubiak M., et al. 1998, Acta As-
tron., 47, 319
Wesselink A.J. 1961, MNRAS, 122, 503
Westerlund B.E. 1990, A&AR, 2, 29